ChemComm

COMMUNICATION

View Article Online
View Journal | View Issue

Cite this: *Chem. Commun.*, 2019, **55**, 14733

Received 20th September 2019,
Accepted 14th November 2019

DOI: 10.1039/c9cc07415e

rsc.li/chemcomm

Selective and reversible interconversion of nanosliders commanded by remote control *via* metal-ion signaling†

Suchismita Saha, Pronay Kumar Biswas, Indrajit Paul and Michael Schmittel *

A multi-device network mainly consisting of two two-component nanosliders was formed by self-sorting of six components. Addition/removal of zinc(II) ions reversibly reorganized the network by chemical signaling involving the translocation of copper(I) from a relay station followed by the selective disassembly/assembly of one of both multi-component devices. The thus liberated machine parts served to erect a three-component nanoslider alongside the other unchanged two-component nanoslider.

Whereas life vitally depends on biocybernetic regulation,[1,2] the networking of artificial molecular devices is still in its infancy.[3–9] It is a great promise of interdependent multi-component ensembles to pave the way toward autonomous and self-regulating systems, *i.e.*, for realizing properties that exceed by far what individual molecules can achieve.

In order to network stand-alone molecular[10–12] or supramolecular[13–20] devices, the functional entities need to be linked by fast chemical communication without harmful interference. All receptors and emitters involved in communication thus need to be highly dynamic and selective with regard to signal uptake, information processing and signal release (= output). The first examples of networked ensembles allowing ON/OFF switchable catalysis have surfaced recently.[21–24] In their key step, a nanoswitch transmitted a defined chemical signal to a functional device (*e.g.*, nanoswitch, nanorotor, or fluorescent receptor) in response to a trigger input. Herein, we demonstrate how a remote control commands the transformation of one nanodevice into another one using the sequential translocation of more than one chemical signal.

In detail, we describe six- and seven-component networks that allow the reversible parallel interconversion of nanosliders. Upon addition of three equiv. of Zn^{2+} to 3 × $[Cu(\mathbf{S})]^+$ (Fig. 1a and b) the equivalent amount of Cu^+, initially deeply buried in nanoswitch $[Cu(\mathbf{S})]^+$, will be translocated from **S** to the free phenanthroline sites of deck **D2**. In essence, the trigger signal commands a remote control unit to emit a chemical signal as second messenger. The ensuing complex $[Cu_3(\mathbf{D2})]^{3+}$ now instructs the nanoslider **M1** = **D1**·**A1** to disassemble and to transfer its biped **A1** for enabling the assembly of the device **M2** = $[Cu_3(\mathbf{D2})(\mathbf{A1})]^{3+}$. In other words, a single input (Zn^{2+}) is sufficient for the parallel dismantling and production of nanodevices through successive two-component translocation. To underline the potential of the concept, the network was furthermore extended to a seven-component system, in which the second translocation had to occur selectively with one out of two bipeds (Fig. 1c).

To probe the required self-sorting, a small set of model studies with various substituted pyridines was undertaken. It turned out that picoline **3** was the optimal terminus in the biped, as it cleanly formed complex **1**·**3** at a 1 : 1 : 1 ratio of zinc porphyrin **1**, phenanthroline **2** and picoline **3**. In contrast, **3** did bind predominantly to **2** in the form of $[Cu(\mathbf{2})(\mathbf{3})]^+$ through HETPYP-I (HETeroleptic PYridine and Phenanthroline)[25,26] complexation when one equiv. of Cu^+ was present (Fig. S9, ESI†).[27] The bulky aryl groups at the 2,9-position of phenanthroline **2** are needed to prevent homoleptic metal complexation.[28,29] The methyl substitution in 2-picoline **3** caused weak binding at the zinc(II) porphyrin ($\log K = 2.72$)[30] whereas the $N_{pic} \rightarrow [Cu(\mathbf{2})]^+$ complexation was strengthened ($\log K = 3.43$).[27]

Thus, the tris(zinc porphyrin) deck **D1**, tris-phenanthroline deck **D2** and the picoline-terminated biped **A1** were selected (Fig. 1a). Due to the anticipated stronger binding of biped **A1** to the Cu^+-loaded phenanthroline deck **D2** than to porphyrin deck **D1**, it was expected that **A1** would prefer binding to $[Cu_3(\mathbf{D2})]^{3+}$. **D2** was synthesized by Sonogashira coupling of 2,9-diaryl-3-ethynyl-1,10-phenanthroline and 1,3,5-tris(4-iodophenyl)benzene (ESI†).

The 1 : 1 mixture of **D1** and **A1** in CD_2Cl_2 is known to quantitatively afford the two-component nanoslider **M1** = **D1**·**A1** where the picoline feet of the biped are axially bound to the zinc(II) porphyrins of the deck (Fig. 1b).[31] As described earlier, due to axial binding, protons t-H and β-H of the tris-porphyrin deck and

Center of Micro and Nanochemistry and Engineering, Organische Chemie I, Universität Siegen, Adolf-Reichwein-Str. 2, D-57068 Siegen, Germany.
E-mail: schmittel@chemie.uni-siegen.de; Tel: +49(0) 2717404356

† Electronic supplementary information (ESI) available: Experimental procedures, compound characterizations, spectral data, UV-vis titrations and computational data. See DOI: 10.1039/c9cc07415e

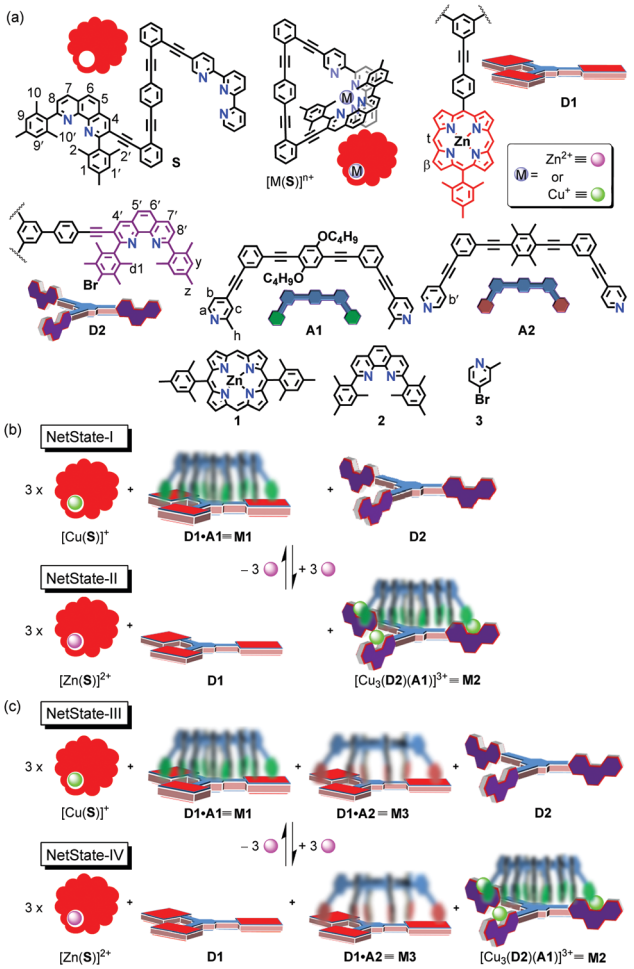

Fig. 1 (a) Chemical structures of switch **S**, decks **D1** and **D2** and bipeds **A1** and **A2** along with their cartoon representations and those of ligands **1**, **2** and **3**. (b) Cartoon representation of the reversible interconversion of nanosliders in NetState-I and NetState-II by addition and removal of Zn^{2+}. (c) Cartoon representation of the selective and reversible interconversion of nanosliders in NetState-III and NetState-IV by addition and removal of Zn^{2+}.

protons a-H, b-H and c-H of the biped arm **A1** diagnostically move upfield.[30] The exchange of the biped between the three zinc porphyrin sites occurs at an exchange frequency of k_{298} = 440 kHz.[31]

Formation of the slider-on-deck **M2** simply required mixing of **D2**, **A1** and $[Cu(CH_3CN)_4]PF_6$ (1 : 1 : 3) in CD_2Cl_2, as confirmed by the upfield shifts of protons a-H, b-H, and c-H of **A1** from 8.48, 7.21, and 7.28 ppm to 7.54, 7.11, and 7.17 ppm, respectively (Fig. 2a). Upfield shifts of protons y-H, d1-H, and z-H from 7.02, 2.53, and 2.36 ppm in the case of $[Cu_3(\mathbf{D2})]^{3+}$ to 6.87, 2.37, and 2.23 ppm in **M2**, respectively, corroborated the biped binding at the metal phenanthroline stations (Fig. 2a and Fig. S19, ESI†). Due to the HETPYP-I binding, these protons were placed in the shielding zone of the π-ring current.[27] The occurrence of a single set of all phenanthroline protons suggested fast exchange of **A1** between all three phenanthroline stations of $[Cu_3(\mathbf{D2})]^{3+}$. To determine the exchange frequency, VT-^{1}H NMR of **M2** was performed which exhibited splitting and a 2 : 1 ratio of various phenanthroline protons (4′-H, 5′-H, 6′-H, 7′-H) at lower temperature (−50 °C).

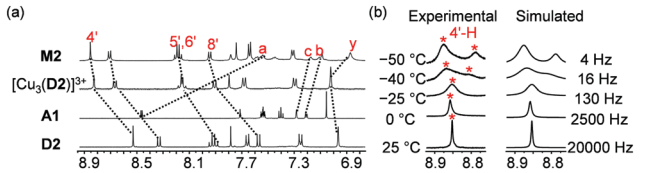

Fig. 2 (a) Partial ^{1}H NMR (400 MHz, CD_2Cl_2, 298 K) of **D2**, **A1**, $[Cu_3(\mathbf{D2})]^{3+}$ and **M2** = $[Cu_3(\mathbf{D2})(\mathbf{A1})]^{3+}$. (b) VT-^{1}H NMR (600 MHz, CD_2Cl_2) of **M2** showing the splitting of 4′-H in a 1 : 2 ratio.

The more downfield signals were assigned to the HETPYP-I complexed phenanthroline sites and the upfield ones to the Cu^+-loaded phenanthroline station (Fig. S30, ESI†). To calculate the exchange frequency of **M2**, the splitting of proton 4′-H was analyzed which at 25 °C appeared as a sharp singlet at 8.86 ppm but split at −50 °C into two sets in a 2 : 1 ratio with a strong coalescence around −40 °C (Fig. 2b). Exchange frequencies (k) at different temperatures were calculated using WinDNMR[32] which provided k_{298} = 20 kHz. Activation parameters were derived from the Eyring plot as $\Delta H^{\ddagger}$ = 61.5 kJ mol^{-1}, $\Delta S^{\ddagger}$ = 44.7 J mol^{-1} K^{-1} and $\Delta G^{\ddagger}_{298}$ = 48.2 kJ mol^{-1} (Table 1 and Fig. S31, ESI†). A single peak at m/z = 915.2 (tri-charged) in ESI-MS confirmed the identity of **M2** (Fig. S36, ESI†), which was additionally supported by a single set of diffusion signals in the ^{1}H–^{1}H DOSY (Fig. S32, ESI†).

After successful formation of both nanosliders, our next intention was to control the reversible and alternate formation of **M1** and **M2** by remote control *via* Cu^+ as a signal. For this purpose, the triangular nanoswitch **S** was selected as a relay because of its ability to capture Cu^+ selectively in the presence of the free deck **D2** and to rather rapidly release Cu^+ onto **D2** upon addition of Zn^{2+}. Nanoswitch **S**, its Cu^+ and Zn^{2+} complexes were unambiguously characterized by ^{1}H NMR, ^{1}H–^{1}H COSY, ESI-MS and elemental analysis (ESI†). Upon complexation with metal ions, protons 1-H, 9-H, 2-H and 10-H split in a 1 : 1 ratio and moved upfield, with the shift being more manifest in $[Zn(\mathbf{S})]^{2+}$ than in $[Cu(\mathbf{S})]^+$ (Fig. 3 and Fig. S14, ESI†). In contrast, protons 4-H, 5-H, 6-H, 7-H and 8-H shifted downfield, again more pronouncedly in $[Zn(\mathbf{S})]^{2+}$ than in $[Cu(\mathbf{S})]^+$ (Fig. 3).

Finally the self-sorting of NetState-I was tested. Nanoswitch **S**, the decks **D1**, **D2**, biped **A1** and Cu^+ were mixed (3 : 1 : 1 : 1 : 3) in CD_2Cl_2 to furnish quantitatively 3 × $[Cu(\mathbf{S})]^+$, **M1** and free **D2** (Fig. 1b). Addition of 3.0 equiv. of Zn^{2+} to NetState-I afforded thrice complex $[Zn(\mathbf{S})]^{2+}$ thus liberating 3.0 equiv. of Cu^+ which translocated to the three phenanthroline sites of **D2** with the effect that biped **A1** shifted from **M1** to $[Cu_3(\mathbf{D2})]^{3+}$ generating NetState-II. NetState-II was reversed back to NetState-I by addition of 3.0 equiv. of hexacyclen. Two complete cycles between NetState-I and NetState-II were performed to demonstrate the reversible nature of the networked system (Fig. S26, ESI†).

Table 1 Exchange frequencies of **M1** and **M2** along with their activation parameters

Nanomachine	k_{298}/kHz	$\Delta H^{\ddagger}$/kJ mol^{-1}	$\Delta S^{\ddagger}$/J K^{-1} mol^{-1}	$\Delta G^{\ddagger}$/kJ mol^{-1}
M1[31]	440[31]	42.9 ± 0.6	7.5 ± 2.5	40.7 ± 0.2
M2	20	61.5 ± 1.0	44.7 ± 4.4	48.2 ± 0.4

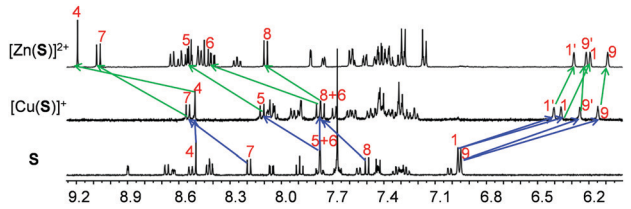

Fig. 3 Partial ^{1}H NMR (400 MHz, CD_2Cl_2, 298 K) of **S**, $[Cu(\mathbf{S})]^+$ and $[Zn(\mathbf{S})]^{2+}$.

Quantitative formation and interconversion of NetStates-I & II was proven by ^{1}H NMR through comparison with data of the individually prepared devices (Fig. 4a). The fabrication of NetState-II was further confirmed by ESI-MS (Fig. S38, ESI†). Protons 1-H, 1′-H, 9-H and 9′-H of **S** with their characteristic ^{1}H NMR signals for $[Cu(\mathbf{S})]^+$ and $[Zn(\mathbf{S})]^{2+}$ allowed tracking of the metal exchange at nanoswitch **S** whereas protons t-H of **D1** and y-H of **D2** showed peak shifts being diagnostic for the formation of **M1** and **M2** (Fig. 4).

The kinetics of the interconversion NetState-I ⇆ II was monitored by UV-vis spectroscopy. As there are negligible shifts in the Soret and Q bands of the zinc porphyrins in **D1** during the detachment/attachment of the biped, changes were monitored at the HETPYP-I complexation site in **D2**, *i.e.*, at the $[Cu(phenAr_2)(pic)]^+$ linkage. Upon changing from NetState-I → NetState-II, the absorptions at 339 and 357 nm disappeared with simultaneous increase of a peak at 386 nm due to formation of **M2** (Fig. 4b). The peaks at 339 and 357 nm were assigned to transitions of the phenanthroline residues whereas the absorption at 386 nm was attributed to the MLCT band of the HETPYP-I complex. Reciprocally, in the NetState-II → I conversion, new peaks at 339 and 357 nm emerged along with the disappearance of the absorbance at 386 nm in agreement with breaking up the HETPYP-I complexation in **M2** (Fig. S44, ESI†).

Absorbance changes at 339 nm were monitored for both the forward and backward process with time (Fig. 4b and Fig. S45, ESI†). Forward conversion (*i.e.*, NetState-I → II, $c = 10^{-6}$ M) took 60 min for completion whereas the backward process (*i.e.*, NetState-II → I) was finished within 12 min. The slow forward process was accelerated by adding iodide as a nucleophile.[33,34] For instance, addition of 3.0 equiv. of iodide sped up the forward transformation (conversion took 12 min) without affecting the rate of the backward process (Fig. S47 and S49, ESI†).

Since the rate determining step in the forward process is the replacement of Cu^+ in $[Cu(\mathbf{S})]^+$ by Zn^{2+}, iodide is supposed to facilitate opening of the switch by coordination to the Cu^+ ion. In the backward process, the rate determining step involves removal of zinc(II) from $[Zn(\mathbf{S})]^{2+}$ by hexacyclen. Since hexacyclen is itself a good nucleophile and in addition the chelate ligand for Zn^{2+} the effect of added iodide is minor.

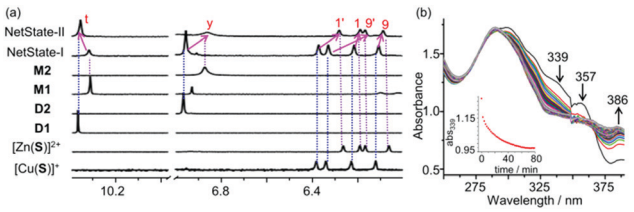

Fig. 4 (a) Partial ^{1}H NMR (400 MHz, CD_2Cl_2) of $[Cu(\mathbf{S})]^+$, $[Zn(\mathbf{S})]^{2+}$, **D1**, **D2**, **M1**, **M2**, NetState-I and NetState-II. (b) UV-vis spectra showing conversion of NetState-I to NetState-II in CH_2Cl_2 (298 K, $c = 10^{-6}$ M) over time. Inset: Changes in absorbance at 339 nm with time.

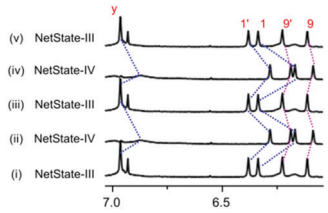

Fig. 5 Partial ^{1}H NMR (400 MHz, CD_2Cl_2, 298 K) shows the reversible interconversion of NetState-III and NetState-IV over two complete cycles. (i) After mixing **S**, **D1**, **D2**, **A1**, **A2** and Cu^+ in a 3 : 2 : 1 : 1 : 1 : 3 ratio (NetState-III). (ii) Addition of 3.0 equiv. of Zn^{2+} to (i). (iii) Addition of 3.0 equiv. of hexacyclen to (ii). (iv) Addition of 3.0 equiv. of Zn^{2+} to (iii). (v) Addition of 3.0 equiv. of hexacyclen to (iv).

To demonstrate biped selectivity in the remote control of the interconverting nanodevices, the complexity was increased by adding the nanoslider **M3** = **D1**·**A2**. This nanodevice (k_{298} = 32.2 kHz) has been described and fully characterized in a previous publication.[31]

In Netstate-III we thus assembled $[Cu(\mathbf{S})]^+$, nansliders **M1**, **M3** and free deck **D2** (Fig. 1c) by self-sorting of nanoswitch **S**, $[Cu(CH_3CN)_4]PF_6$, deck **D1**, bipeds **A1** and **A2** and phenanthroline deck **D2** (3 : 3 : 2 : 1 : 1 : 1). Analysis of the ^{1}H NMR confirmed formation of **M1** and **M3** by the characteristic upfield shifts of protons c-H, h-H and b′-H at 6.16, −0.14 and 5.45 ppm, respectively (Fig. S27, ESI†). In addition, characteristic signals for 1-H, 1′-H, 9-H and 9′-H of $[Cu(\mathbf{S})]^+$ and y-H of free **D2** substantiated the quantitative formation of NetState-III. Addition of 3.0 equiv. of $Zn(OTf)_2$ translocated the Cu^+ ions from $[Cu(\mathbf{S})]^+$ to the free phenanthroline sites of deck **D2**. The resultant $[Cu_3(\mathbf{D2})]^{3+}$ has now the option to claim either biped **A1** or **A2** for generating either **M2** or **M4** = $[Cu_3(\mathbf{D2})(\mathbf{A2})]^{3+}$. Selective translocation of **A1** was proven by the upfield shift of protons y-H, z-H and d1-H at 6.87, 2.23 and 2.37 ppm, respectively, exactly matching with the signals for **M2** (Fig. S28, ESI†). If **A2** had been translocated fabricating **M4** = $[Cu_3(\mathbf{D2})(\mathbf{A2})]^{3+}$, the above mentioned peaks should have shifted to 7.02, 2.39 and 2.57 ppm, respectively (Fig. S21, ESI†). Quantitative formation of **M2** over **M4** in NetState-IV was supported by the ESI-MS (Fig. S39, ESI†). Two complete cycles between NetState-III and NetState-IV proved the reversibility and selectivity of the seven-component networked system (Fig. 5).

In conclusion, we have demonstrated a six-component cybernetic network of a triangular switch controlling the self-assembly of two alternate nansliders *via* chemical signaling.[35] In this network, a single chemical input (Zn^{2+} or hexacyclen) controls two consecutive translocations (of Cu^+ ion and sliding biped **A1**) which lead to the alternate assembly/disassembly of two nansliders. Furthermore, the observed selectivity in the second translocation, *i.e.*, that of biped **A1**, demonstrated a high level of control in the seven-component system. Two complete cycles of the assembly/disassembly of nansliders proved the

reversibility of the cybernetic process. The kinetics of translocation was controlled by addition of iodide.

In summary, this manifestation of remote control is a decisive step toward supramolecular systems chemistry integrating multiple stand-alone supramolecular devices into higher-order multicomponent nanomachinery. Using furthermore chemical fuel in such domino translocations should lead to interesting off-equilibrium[36–42] applications.

We are indebted to the Deutsche Forschungsgemeinschaft for continued support under Schm 647/19-2 and 647/20-2. We thank Dr Paululat for measuring the VT-^{1}H NMR. Dedicated to Prof. Dr J.-P. Sauvage on the occasion of his 75th birthday and with deep gratitude for his inspiring and groundbreaking work.

Conflicts of interest

There are no conflicts to declare.

Notes and references

1 B. Korzeniewski, *J. Theor. Biol.*, 2001, **209**, 275–286.
2 A. Bielecki, *Biol. Cybern.*, 2015, **109**, 401–419.
3 M. Barboiu and J.-M. Lehn, *Proc. Natl. Acad. Sci. U. S. A.*, 2002, **99**, 5201–5206.
4 M. Barboiu, G. Vaughan, N. Kyritsakas and J.-M. Lehn, *Chem. – Eur. J.*, 2003, **9**, 763–769.
5 D. Ray, J. T. Foy, R. P. Hughes and I. Aprahamian, *Nat. Chem.*, 2012, **4**, 757–762.
6 S. Pramanik, S. De and M. Schmittel, *Angew. Chem., Int. Ed.*, 2014, **53**, 4709–4713.
7 S. Pramanik, S. De and M. Schmittel, *Chem. Commun.*, 2014, **50**, 13254–13257.
8 A.-M. Stadler, L. Karmazin and C. Bailly, *Angew. Chem., Int. Ed.*, 2015, **54**, 14570–14574.
9 S. Pramanik and I. Aprahamian, *J. Am. Chem. Soc.*, 2016, **138**, 15142–15145.
10 V. Balzani, A. Credi and M. Venturi, *Chem. Soc. Rev.*, 2009, **38**, 1542–1550.
11 S. Erbas-Cakmak, D. A. Leigh, C. T. McTernan and A. L. Nussbaumer, *Chem. Rev.*, 2015, **115**, 10081–10206.
12 S. Kassem, T. van Leeuwen, A. S. Lubbe, M. R. Wilson, B. L. Feringa and D. A. Leigh, *Chem. Soc. Rev.*, 2017, **46**, 2592–2621.
13 J. D. Badjic, V. Balzani, A. Credi, S. Silvi and J. F. Stoddart, *Science*, 2004, **303**, 1845–1849.
14 S. Hiraoka, E. Okuno, T. Tanaka, M. Shiro and M. Shionoya, *J. Am. Chem. Soc.*, 2008, **130**, 9089–9098.
15 M. L. Saha, S. Neogi and M. Schmittel, *Dalton Trans.*, 2014, **43**, 3815–3834.
16 M. Schmittel, *Chem. Commun.*, 2015, **51**, 14956–14968.
17 Y. Takara, T. Kusamoto, T. Masui, M. Nishikawa, S. Kume and H. Nishihara, *Chem. Commun.*, 2015, **51**, 2896–2898.
18 P. K. Biswas, S. Saha, T. Paululat and M. Schmittel, *J. Am. Chem. Soc.*, 2018, **140**, 9038–9041.
19 M. Schmittel and S. Saha, *Adv. Inorg. Chem.*, 2018, **71**, 135–176.
20 A. Goswami and M. Schmittel, *Coord. Chem. Rev.*, 2018, **376**, 478–505.
21 N. Mittal, S. Pramanik, I. Paul, S. De and M. Schmittel, *J. Am. Chem. Soc.*, 2017, **139**, 4270–4273.
22 A. Goswami, S. Pramanik and M. Schmittel, *Chem. Commun.*, 2018, **54**, 3955–3958.
23 S. Gaikwad, S. Pramanik, S. De and M. Schmittel, *Dalton Trans.*, 2018, **47**, 1786–1790.
24 I. Paul, N. Mittal and M. Schmittel, *J. Am. Chem. Soc.*, 2019, **141**, 5139–5143.
25 S. Neogi, Y. Lorenz, M. Engeser, D. Samanta and M. Schmittel, *Inorg. Chem.*, 2013, **52**, 6975–6984.
26 S. Neogi, G. Schnakenburg, Y. Lorenz, M. Engeser and M. Schmittel, *Inorg. Chem.*, 2012, **51**, 10832–10841.
27 N. Mittal, M. S. Özer and M. Schmittel, *Inorg. Chem.*, 2018, **57**, 3579–3586.
28 M. Schmittel, C. Michel, S.-X. Liu, D. Schildbach and D. Fenske, *Eur. J. Inorg. Chem.*, 2001, 1155–1166.
29 K. Mahata and M. Schmittel, *J. Am. Chem. Soc.*, 2009, **131**, 16544–16554.
30 A. Ghosh, I. Paul, S. Saha, T. Paululat and M. Schmittel, *Org. Lett.*, 2018, **20**, 7973–7976.
31 I. Paul, A. Goswami, N. Mittal and M. Schmittel, *Angew. Chem., Int. Ed.*, 2018, **57**, 354–358.
32 H. J. Reich, *J. Chem. Educ., Software*, 1996, **3D**, 2.
33 A. Livoreil, J.-P. Sauvage, N. Armaroli, V. Balzani, L. Flamigni and B. Ventura, *J. Am. Chem. Soc.*, 1997, **119**, 12114–12124.
34 S. Saha, P. K. Biswas and M. Schmittel, *Inorg. Chem.*, 2019, **58**, 3466–3472.
35 P. Remón and U. Pischel, *ChemPhysChem*, 2017, **18**, 1667–1677.
36 C. Cheng, P. R. McGonigal, S. T. Schneebeli, H. Li, N. A. Vermeulen, C. Ke and J. F. Stoddart, *Nat. Nanotechnol.*, 2015, **10**, 547–553.
37 C. S. Wood, C. Browne, D. M. Wood and J. R. Nitschke, *ACS Cent. Sci.*, 2015, **1**, 504–509.
38 M. R. Wilson, J. Solà, A. Carlone, S. M. Goldup, N. Lebrasseur and D. A. Leigh, *Nature*, 2016, **534**, 235–240.
39 B. S. L. Collins, J. C. M. Kistemaker, E. Otten and B. L. Feringa, *Nat. Chem.*, 2016, **8**, 860–866.
40 J. A. Berrocal, C. Biagini, L. Mandolini and S. Di Stefano, *Angew. Chem., Int. Ed.*, 2016, **55**, 6997–7001.
41 S. Erbas-Cakmak, S. D. P. Fielden, U. Karaca, D. A. Leigh, C. T. McTernan, D. J. Tetlow and M. R. Wilson, *Science*, 2017, **358**, 340–343.
42 A. Ghosh, I. Paul, M. Adlung, C. Wickleder and M. Schmittel, *Org. Lett.*, 2018, **20**, 1046–1049.

